

Enantioselective manipulation of single chiral nanoparticles using optical tweezers

R. Ali,* F. A. Pinheiro, F. S. S. Rosa, and P. A. Maia Neto
*Instituto de Física, Universidade Federal do Rio de Janeiro,
 Caixa Postal 68528, Rio de Janeiro, RJ, 21941-972, Brasil*

R. S. Dutra
*LISComp-IFRJ, Instituto Federal de Educação, Ciência e Tecnologia,
 Rua Sebastião de Lacerda, Paracambi, RJ, 26600-000, Brasil
 (Dated: January 7, 2022)*

We put forward an enantioselective method for chiral nanoparticles using optical tweezers. We demonstrate that the optical trapping force in a typical, realistic optical tweezing setup with circularly-polarized trapping beams is sensitive to the chirality of core-shell nanoparticles, allowing for efficient enantioselection. It turns out that the handedness of the trapped particles can be selected by choosing the appropriate circular polarization of the trapping beam. The chirality of each individual trapped nanoparticle can be characterized by measuring the rotation of the equilibrium position under the effect of a transverse Stokes drag force. We show that the chirality of the shell gives rise to an additional twist, leading to a strong enhancement of the optical torque driving the rotation. Both methods are shown to be robust against variations of size and material parameters, demonstrating that they are particularly useful in (but not restricted to) several situations of practical interest in chiral plasmonics, where enantioselection and characterization of single chiral nanoparticles, each and every with its unique handedness and optical properties, are in order. In particular, our method could be employed to unveil the chiral response arising from disorder in individual plasmonic raspberries, synthesized by close-packing a large number of metallic nanospheres around a dielectric core.

The concept of chirality, introduced by Lord Kelvin to designate any geometrical object or ensemble of points that lack mirror symmetry, is ubiquitous in Nature [1]. Chirality is essential in several nanotechnological applications [2]. Plasmonic structures provide a promising material platform for artificially designed chiral systems and applications [3–5]. One of the major goals of the emerging field of chiral plasmonics is to tailor optical chiral responses orders of magnitude larger than those of natural chiral materials.

Indeed, new classes of chiral systems composed of plasmonic nanoparticles have been recently developed. Examples include achiral metallic particles arranged in chiral geometries, such as helices [6] or random configurations [7], chiral metallic nanocrystals [8], DNA-assembled plasmonic nanostructures [9, 10], chiral plasmonic particles assembled on scaffolds [11], and core-shell plasmonic spheres [12, 13]. However, the handedness and geometrical chirality of many of these artificial plasmonic structures, which ultimately govern the optical chiral response, are not *a priori* known after the nanofabrication process. Besides, many applications involve single, isolated chiral nanoparticles, each one with unique, unknown handedness, geometry and optical properties. In these cases, traditional probes of chirality, such as rotatory power and circular dichroism [14], are expected to fail in probing single-particle properties as they typically provide an average chiral response of these structures in solution.

Here we propose using optical tweezers (OT) [15] with a single circularly-polarized trapping beam to select and probe the handedness of single, isolated chiral nanoparticles. By applying for the first time optical tweezers to plasmonic particles, we demonstrate all-optical enantioselection and manipulation of an important class of materials in chiral plasmonics, namely core-shell metallic chiral nanoparticles, which are an excellent model for metal-organic nanoparticles with strong optical activity [12]. In our proposal, sketched in Fig. 1(a), a circularly-polarized Gaussian laser beam propagating along the z -direction reaches an oil immersion high-NA objective that focuses the beam into a diffraction-limited spot in the sample beyond the coverslip. The sample contains chiral nanoparticles dispersed in water. We show that optical trapping can only occur for particles with the handedness selected by the choice of the trapping beam circular polarization, thus allowing for enantioselectivity.

Our proposal is simpler than previous optical chiral resolution methods [16–32], including those which have been experimentally implemented [33–40]. More importantly, it allows for a quantitative measurement of the chirality parameter κ of single, individual nanoparticles, an important task that to the best of our knowledge has never been achieved so far [64]. For that purpose, we drive the sample laterally and measure the resulting rotation angle α of the equilibrium position shown in Fig. 1. As illustrated by Fig. 1(b), the rotation around the laser beam axis z is a consequence of the optical torque produced by the azimuthal optical force component F_ϕ exerted on the trapped microsphere when the latter is displaced off-axis by the Stokes drag force F_S .

*r.ali@if.ufrj.br

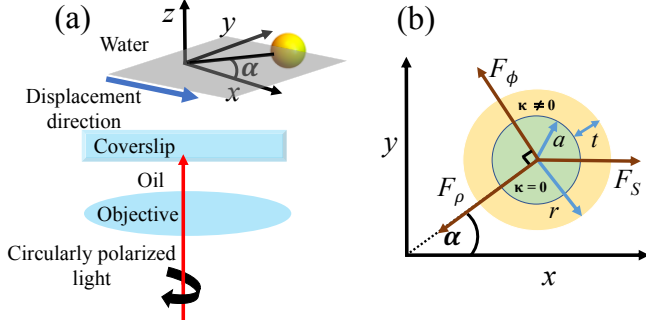


FIG. 1: (a) Schematic representation of the proposed enantioselection with optical tweezers. A circularly-polarized Gaussian laser beam is focused into a spot at the focal plane of a high-NA objective, trapping core-shell nanospheres in the aqueous solution. The handedness of the chiral shell allowing for trapping is selected by choosing the appropriate circular polarization. In order to provide for further enantioselectivity and characterization of the chirality parameter, the trapped nanosphere is displaced off-axis by driving the sample along the x direction with a constant speed. (b) The resulting Stokes drag force F_S is represented alongside the cylindrical optical force components F_ρ and F_ϕ . The latter accounts for the OAM transferred to the nanosphere. The equilibrium position is rotated around the z -axis by the angle α .

In other words, F_ϕ accounts for the partial transfer of optical angular momentum to the trapped particle and its sign is controlled by the optical helicity.

More specifically, the rotation angle at equilibrium α is found from $\tan \alpha = F_\phi / |F_\rho|$, where $F_\rho < 0$ is the restoring radial optical force also depicted in Fig. 1(b). Due to the symmetry of the beam profile, both F_ϕ and F_ρ are independent of the angular position of the sphere.

For achiral homogenous microspheres, the angle of rotation α was measured and compared with theory [41]. It turns out, as we show below, that for chiral shells α is considerably larger than the typical values measured in [41], indicating that our proposal can indeed be implemented experimentally. In addition, we show that α is strongly dependent on the shell chirality parameter κ , allowing for a determination of κ from the measurement of α .

A general formalism of optical torques on chiral particles was developed in Ref. [42]. Here we compute the optical torque and the resulting rotation angle by extending the Mie-Debye with Spherical Aberration (MDSA) theory of optical tweezers [43–46] to encompass the case of nanospheres with a chiral coating. Our theoretical construction consists of three steps: (i) start from a realistic non-paraxial description of the highly-focused trapping beam, taking into account the spherical aberration introduced by refraction at the interface between the coverslip and the sample; (ii) derive the scattered field by taking the representation for the focused beam obtained in (i) as the incident field on a sphere coated with a chiral layer; and (iii) integrate the resultant Maxwell stress

tensor over an appropriate Gaussian surface to derive the optical force. An alternative theory of optical tweezers for homogeneous chiral particles and clusters based on the T-matrix formalism has recently appeared [47].

Step (i) is based on the non-paraxial Debye model of a focused beam, later extended in Ref. [48] to account for polarization. We also introduce the spherical aberration effect by following Ref. [49]. Step (ii) requires an extension of MDSA involving a description of chiral media. In their most simple and useful instance, the constitutive equations [50] mixing the electric field \mathbf{E} , the electric displacement \mathbf{D} , the magnetic field \mathbf{B} and the auxiliary field \mathbf{H} for a chiral medium are given by [51, 52]

$$\begin{aligned} \mathbf{D}(\mathbf{r}, \omega) &= \epsilon_0 \epsilon(\omega) \mathbf{E}(\mathbf{r}, \omega) + i\sqrt{\epsilon_0 \mu_0} \kappa(\omega) \mathbf{H}(\mathbf{r}, \omega), \\ \mathbf{B}(\mathbf{r}, \omega) &= -i\sqrt{\epsilon_0 \mu_0} \kappa(\omega) \mathbf{E}(\mathbf{r}, \omega) + \mu_0 \mu(\omega) \mathbf{H}(\mathbf{r}, \omega), \end{aligned} \quad (1)$$

where ϵ and μ are the relative permittivity and permeability of the medium (ϵ_0 and μ_0 are the absolute vacuum permittivity and permeability), and κ is the (relative) chirality parameter.

We first write the incident focused beam as a superposition of plane waves, and then solve for the scattering of each plane wave component by following the method of Ref. [53] and imposing the appropriate boundary conditions at each interface of the coated nanosphere. The total scattered field is finally obtained by superposing all scattered components. Finally, the optical force \mathbf{F} is derived by integration of the stress tensor [step (iii)]. Momentum conservation allows one to take a spherical Gaussian surface $S(R)$ at infinity:

$$\mathbf{F} = \lim_{R \rightarrow \infty} \left[-\frac{R}{2} \int_{S(R)} d\Omega \mathbf{r} (\epsilon_0 \epsilon_w E^2 + \mu_0 H^2) \right], \quad (2)$$

where $\epsilon_w = n_w^2$ and n_w is the water refraction index.

The resulting optical force is written as a multipole series in terms of the coefficients

$$\begin{aligned} G_{\ell m}^{(\sigma)}(\rho, z) &= \int_0^{\theta_0} d\theta \sin \theta \sqrt{\cos \theta} e^{-\gamma^2 \sin^2 \theta} d_{m, \sigma}^\ell(\theta_w) T(\theta) \\ &\quad \times e^{i\Phi_w(\theta)} J_{m-\sigma}(k\rho \sin \theta) e^{ik_w \cos \theta_w z}, \end{aligned} \quad (3)$$

which are functions of the sphere position (with respect to the paraxial focus) in cylindrical coordinates (ρ, z) , with ℓ, m representing the multipole order. Explicit expressions for the cylindrical components of \mathbf{F} are given in the supplementary material [54]. We take $\sigma = \pm 1$ for left-handed/right-handed circular polarizations. The integration variable θ represents the angle between each incident propagation direction in the glass medium (index n_g) and the z -axis. The integration limit is defined by the objective numerical aperture (NA): $\theta_0 = \arcsin(\text{NA}/n_g)$. The parameter γ represents the ratio of the objective focal length to the Gaussian beam waist at the objective entrance port (but note that the focused beam is not described by a paraxial Gaussian model). $T(\theta)$ is the Fresnel transmission amplitude for refraction at the interface between the glass coverslip and the aqueous solution.

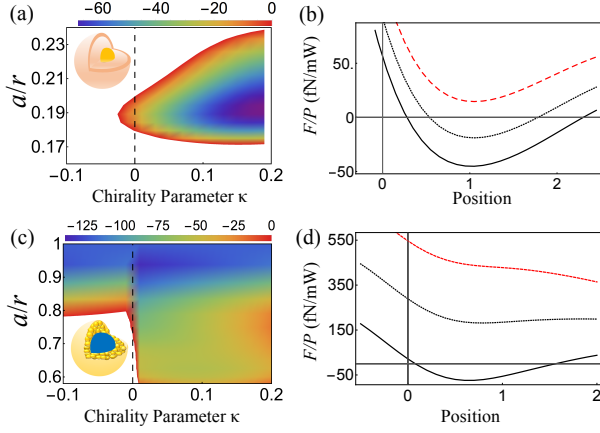


FIG. 2: (a,c) Density plot showing the range of chirality parameter κ and aspect ratio a/r (see Fig. 1) leading to negative axial forces at the position (a) $z/r = 1.3$ and (c) $z/r = 0.5$. The color scale represents the force in femtonewtons for a laser beam power of 1 mW. (b,d) Axial force as a function of position (in units of the sphere outer radius r) for (b) $\kappa = -0.05$ (dash), $\kappa = 0$ (dot), $\kappa = 0.05$ (solid) and (d) $\kappa = -0.05 - 0.007i$ (dash), $\kappa = 0$ (dot), $\kappa = 0.05 + 0.007i$ (solid). Panels (a,b) refer to metal-organic core-shell particles made of a gold core ($a = 70$ nm) coated with a dielectric chiral shell, whereas (c,d) correspond to raspberry-like core-satellite particles made of several layers of metallic nanospheres randomly distributed around a silica core (radius $a = 300$ nm). The outer radius is $r = 370$ nm and 450 nm in panels (b) and (d), respectively. In all cases we take a left-handed circularly-polarized laser beam.

Such refraction also introduces the spherical aberration phase correction $\Phi_w(\theta)$. Explicit expressions are given in [54]. $d_{m,m'}^l(\theta_w)$ are the Wigner rotation matrix elements [55] evaluated at the angle $\theta_w = \arcsin(n_g \sin \theta / n_w)$ in the aqueous solution and J_m are the cylindrical Bessel functions of integer order m [3]. Finally, $k = 2\pi n_g / \lambda_0$ and $k_w = n_w k / n_g$ are the wavenumbers in the glass and aqueous solution, respectively, where λ_0 is the vacuum wavelength.

For all numerical examples discussed below, we take the typical values [57] $\lambda_0 = 1064$ nm, $n_w = 1.332$, $n_g = 1.51$, $\gamma = 1.226$ and $\text{NA} = 1.3$. We take right-handed circular polarization ($\sigma = -1$), but results for the opposite helicity $\sigma = 1$ can be trivially obtained from those shown here by changing the signs of both α and κ . We consider different realistic examples of core-shell nanospheres of both technological and scientific interest. We start with metal-organic nanoparticles [12] consisting of a gold core (radius $a = 70$ nm) and a dielectric chiral shell with a relative permittivity $\epsilon_s = 2.89$. Fig. 2(a) presents a density plot showing the negative (backward) values of the axial force F_z , required for trapping, as function of the chirality parameter κ and the aspect ratio a/r (r = outer radius). Numerical values are given for the force divided by the laser beam power P in the

sample region. We take the sphere center at the plane $z/r = 1.3$, where $z = 0$ corresponds to the paraxial focal plane. Outside the colored region shown in Fig. 2(a), radiation pressure dominates and the optical force is positive [58], thus expelling the particle from the focal region. Thus, we select right-handed (left-handed) shells by taking $\sigma = -1$ (+1) trapping beams.

To confirm chiral resolution and have further insight into the trapping conditions, we plot in Fig. 2(b) the variation of F_z/P with the axial position of the sphere in units of the outer radius $r = 370$ nm. The particle with $\kappa = 0.05$ (solid) is indeed trapped at a stable equilibrium position close to the focus ($z = 0$), while the force for the opposite value of κ is positive everywhere along the beam axis (dashed), thus flushing the particles with the opposite handedness away from the focal region. For achiral particles (dotted), the optical axial force lies in between the two previous cases, and a less stable trapping is achieved further away from the focal point.

In Figs. 2(c,d) we consider a second example of plasmonic particle, composed of randomly distributed metallic nanoparticles attached to a dielectric spherical core. Such so-called plasmonic “raspberries” are dielectric spheres decorated with metallic nanoparticles that show high optical magnetism [59–63]. Since disorder is known to produce geometries lacking mirror symmetry [7], we discuss here how to characterize the chirality of an individual plasmonic raspberry by employing optical tweezers. We model these structures as core-shell composites with a silica spherical core (radius $a = 300$ nm) coated with homogeneous chiral metallic shells (permittivity $\epsilon_s = 2.89 + 0.03i$). In Fig. 2(c), we show that trapping is enantioselective when the shell thickness t is larger than ~ 100 nm. Those length scales are similar to the size parameters of the multi-layered raspberries reported in Ref. [62]. For a shell thickness $t = 150$ nm, Fig. 2(d) shows that particles with $\kappa = 0.050 + 0.007i$ are trapped (solid), whereas achiral (dotted) or chiral with opposite handedness (dashed) are pushed away from the focal region by radiation pressure.

Our proposal can also be applied outside the domain of chiral plasmonics, as demonstrated in Fig. 3. We consider a core-shell dielectric particle with a silica core of radius $a = 300$ nm and a dielectric chiral shell of permittivity $\epsilon = 2.89$ and thickness t . The axial force variation with position is shown in the main plot of panel (a) for $t = 175$ nm. Stable trapping is achieved for realistic positive values for the chirality parameter κ [64], while nanospheres coated with the opposite handedness are expelled from the focal region as in our previous examples. A more complete picture is provided by the density plot in the inset of 3(a), where the conventions are the same as in Figs. 2(a,c). Enantioselectivity is possible in the range $100 \text{ nm} < t < 200 \text{ nm}$, whereas spheres coated with thin layers ($t < 100 \text{ nm}$) are trapped regardless of the sign of κ , recovering the results for achiral homogeneous nanospheres [43, 44] as $t \rightarrow 0$.

The range of enantioselection can be further extended

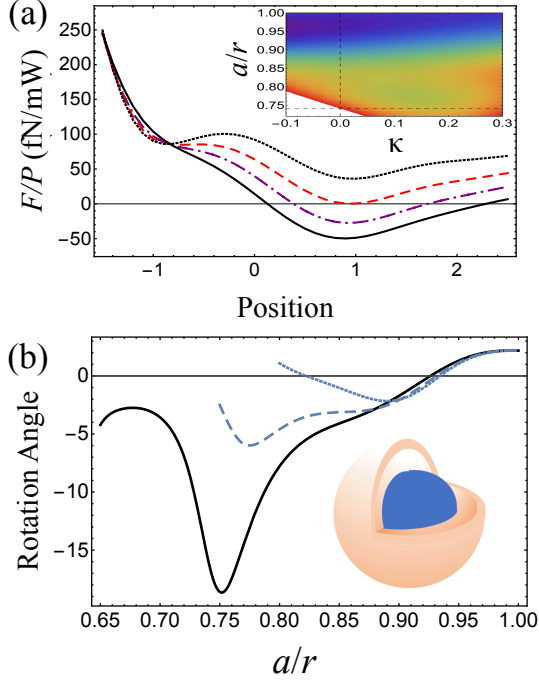


FIG. 3: (a) Axial force as a function of position (in units of the sphere outer radius r) for chirality parameter $\kappa = -0.05$ (dot), $\kappa = 0$ (dash), $\kappa = +0.05$ (dot-dash) and $\kappa = 0.12$ (solid). Inset: density plot showing the range of κ and aspect ratio a/r leading to negative axial forces required for trapping, at the fixed nanosphere position $z/r = 1$. (b) Rotation angle α of the particle equilibrium position as a function of aspect ratio a/r , for chirality parameters $\kappa = 0.12$ (solid), $\kappa = 0$ (dash) and $\kappa = -0.1$ (dot). For the last two cases, the curves end at their respective thresholds of no trapping, since radiation pressure dominates for smaller values of a/r . In all panels, we consider a silica core of radius $a = 300$ nm and a dielectric chiral shell with $\epsilon_s = 2.89$. The shell thickness is $t = 375$ nm in the main plot of panel (a).

into the thickness interval $40 \text{ nm} \lesssim t \lesssim 100 \text{ nm}$ by driving the sample laterally so as to displace the trapped particle away from the beam axis, as discussed in connection with Fig. 1. Due to the transfer of optical angular momentum (OAM), the equilibrium position is rotated by an angle α around the beam axis. In Fig. 3(b), we plot α as a function of the aspect ratio a/r . For thin shells corresponding to aspect ratios in the range $0.88 \gtrsim a/r \gtrsim 0.74$, the curves corresponding to different chiralities are sufficiently far apart to distinguish between shells with positive, negative and vanishing values of κ shown in Fig. 3.

For homogenous achiral spheres, the rotation angle α is usually opposite to the polarization handedness of the trapping beam [41] (so-called negative optical torque [65–67]). Indeed, we find a positive α in the limit $a/r \rightarrow 1$ when taking right-handed circular polarization (negative spin angular momentum) as in the example of Fig. 3(b). On the other hand, Fig. 3 shows that optical torque goes positive when considering thicker chiral shells.

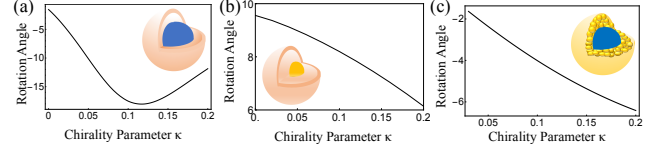


FIG. 4: Rotation angle α of the particle equilibrium position as a function of the chirality parameter κ for (a) dielectric core-shell, (b) metal-organic core-shell and (c) raspberry-like core-satellite particles. The geometrical dimensions in (a,b,c) are the same as in Figs. 3, 2(b) and 2(d), respectively. As in the previous figures, we take left-handed circular polarization. In panel (c), we take $\text{Im}(\kappa) = 0.007$.

The solid line, corresponding to $\kappa = 0.12$, shows that the rotation angle depends strongly on the shell thickness and has a peak value $\alpha \approx 19^\circ$ close to $t = 100$ nm. This is ~ 5 times larger than the typical values predicted and measured for achiral homogeneous particles of similar dimensions [41]. Such an impressive increase makes trapped single spheres with chiral coatings particularly suitable for experimental demonstrations of optical torque in optical tweezers.

The results of Fig. 3(b) suggest that the transfer of OAM in optical tweezers might provide an efficient method for characterizing the thickness of chiral coatings. In fact, the rotation angle also depends strongly on the chirality parameter κ and can be employed to characterize its value for individual particles with a high resolution. In Fig. 4, we plot the rotation angle α as a function of the chirality parameter κ for the three examples we have considered in this letter: (a) a dielectric core-shell with a silica core of radius $a = 300$ nm and a chiral shell of thickness $t = 375$ nm; (b) a metal-organic particle with a gold core of radius $a = 70$ nm and chiral dielectric shell of thickness $t = 300$ nm; and (c) a plasmonic raspberry with a silica core of radius $a = 300$ nm and a chiral metallic shell of thickness $t = 150$ nm. Remarkably, the optical torque is positive for the dielectric and plasmonic raspberry particles, and negative for the metal-organic one. For all three cases, α displays a strong, approximately linear dependence in the range $0 \leq \kappa \lesssim 0.1$, allowing for a good resolution in the determination of κ in this important range. Given a typical precision $\delta\alpha \sim 0.2^\circ$ in the determination of the rotation angle [41], we estimate from Fig. 4 a chirality resolution $\delta\kappa \sim 10^{-3}$ for the dielectric core-shell particle, and $\delta\kappa \sim 10^{-2}$ for the metal-organic and raspberry composites.

As discussed previously, it is also possible to trap nanospheres coated with the opposite handedness by switching to left-handed circular polarization. In this case, the sign of the rotation angle is reversed, and the resulting variation allows for the characterization of negative values of κ .

In conclusion, we have shown that optical tweezing of chiral core-shell nanospheres is enantioselective, since the handedness allowing for trapping can be selected

by choosing the appropriate circular polarization of the laser beam. For the plasmonic raspberry-like and the core-shell dielectric particles, enantioselection is achieved as long as the chiral shell thickness exceeds ~ 100 nm. Nanospheres with the opposite handedness are simply pushed away from the focal region by radiation pressure. In addition, we put forward a method for characterization of the chirality parameter κ based on the rotation of the trapped particle equilibrium position when it is displaced off-axis by driving the sample laterally.

We generally find large rotation angles that should be more easily measurable than in the experiment reported in Ref. [41]. The angle is strongly dependent on the chirality parameter, thus providing a good resolution for its characterization in the range $|\kappa| \lesssim 0.1$. Our method is particularly suited to unveil chirality of plasmonic raspberries, which is expected to exist due to the random arrangement of metallic satellites that lacks mirror symmetry. In contrast to traditional methods to probe chirality, such as circular dichroism and rotatory power, here the chiral optical response does not show up as the average response of particles in suspension, but only when probing individual particles, each one with its unique handed-

ness. Altogether our results demonstrate a twofold mechanism for all-optical manipulation of chiral nanoparticles, based on optical trapping and rotation, paving the way for the investigation of the chiral response of plasmonic nanoparticles and applications.

Acknowledgments

We thank K. Diniz, D. S. Ether Jr, L. B. Pires and N. B. Viana for inspiring discussions. This work has been supported by the Brazilian agencies National Council for Scientific and Technological Development (CNPq), Coordination for the Improvement of Higher Education Personnel (CAPES), the National Institute of Science and Technology Complex Fluids (INCT-FCx), and the Research Foundations of the States of Minas Gerais (FAPEMIG), Rio de Janeiro (FAPERJ) and São Paulo (FAPESP). F. A. P. thanks the Royal Society – Newton Advanced Fellowship (grant no. NA150208) for financial support.

-
- [1] G. H. Wagnière, *On chirality and the universal asymmetry: reflections on image and mirror image*, Wiley-VCH, Zurich, (2007).
 - [2] J. Zhang, M. T. Albelda, Y. Liu, and J. W. Canary, *Chiral nanotechnology*, Chirality **17**, 404 (2005).
 - [3] M. J. Urban, C. Shen, X.-T. Kong, C. Zhu, A. O. Govorov, Q. Wang, M. Hentschel, N. Liu, *Chiral plasmonic nanostructures enabled by bottom-up approaches*, Annual Review of Physical Chemistry **70**, 275 (2019).
 - [4] M. Hentschel, M. Schaferling, X. Duan, H. Giessen, and N. Liu, *Chiral plasmonics*, Science Advances **3**, e1602735 (2017).
 - [5] X.-T. Kong, L. V. Besteiro, Z. Wang, and A. O. Govorov, *Plasmonic chirality and circular dichroism in bioassembled and nonbiological systems: theoretical background and recent progress* Adv.Mater. 1801790 (2018).
 - [6] Z. Fan, A. O. Govorov, *Plasmonic circular dichroism of chiral metal nanoparticle assemblies*, Nano Lett., **10**, 2580 (2010).
 - [7] F. A. Pinheiro, V. A. Fedotov, N. Papasimakis, and N. I. Zheludev, *Spontaneous natural optical activity in disordered media*, Phys. Rev. B **95**, 220201(R) (2017).
 - [8] Z. Fan, A. O. Govorov, *Chiral nanocrystals: plasmonic spectra and circular dichroism*, Nano Lett. **12**, 3283 (2012).
 - [9] A. Kuzyk, R. Schreiber, Z. Fan, G. Pardatscher, E.-M. Roller, A. Hoge, F. C. Simmel, A. O. Govorov, and T. Liedl, *DNA-based self-assembly of chiral plasmonic nanostructures with tailored optical response* Nature, **483** 311 (2012).
 - [10] W.J. Yan *et al.* *Self-assembly of chiral nanoparticle pyramids with strong R/S optical activity*, J. Am. Chem. Soc. **134**, 15114 (2012).
 - [11] A. D. Merg, J. C. Boatz, A. Mandal, G. Zhao, S. Mokashi-Punekar, C. Liu, X. Wang, P. Zhang, P. C. A. Van Der Wel, N. L. Rosi, *Peptide-directed assembly of single-helical gold nanoparticle superstructures exhibiting intense chiroptical activity*, J. Am. Chem. Soc. **138**, 13655 (2016).
 - [12] X. Wu, L. Xu, W. Ma, L. Liu, H. Kuang, W. Yan, L. Wang, C. Xu, *Gold core-DNA-silver shell nanoparticles with intense plasmonic chiroptical activities*, Adv. Funct.Mater. **25**, 850 (2015).
 - [13] W. Liu *et al.*, *Gold nanorod chiral mesoporous silica core-shell nanoparticles with unique optical properties*, Am. Chem. Soc. **135**, 9659 (2013).
 - [14] F. Graf, J. Feis, X. Garcia-Santiago, M. Wegener, C. Rockstuhl and I. Fernandez-Corbaton, *Achiral, Helicity Preserving, and Resonant Structures for Enhanced Sensing of Chiral Molecules*, ACS Photonics, **6**, 482 2019.
 - [15] A. Ashkin, J. M. Dziedzic, J. E. Bjorkholm, and S. Chu, *Observation of a single-beam gradient force optical trap for dielectric particles*, Opt. Lett. **11**, 288 (1986).
 - [16] Y. Li, C. Bruder, and C. Sun, *Generalized Stern-Gerlach effect for chiral molecules*, Phys. Rev. Lett. **99**, 130403 (2007).
 - [17] B. Spivak and A. Andreev, *Photoinduced separation of chiral isomers in a classical buffer gas*, Phys. Rev. Lett. **102**, 063004 (2009).
 - [18] X. Li and M. Shapiro, *Theory of the optical spatial separation of racemic mixtures of chiral molecules*, J. Chem. Phys. **132**, 194315 (2010).
 - [19] R. P. Cameron, S. M. Barnett, and A. M. Yao, *Discriminatory optical force for chiral molecules*, New J. Phys. **16**, 013020 (2014).
 - [20] A. Canaguier-Durand, J. A. Hutchison, C. Genet, and T. W. Ebbesen, *Mechanical separation of chiral dipoles by chiral light*, New J. Phys. **15**, 123037 (2013).

- [21] D. S. Bradshaw and D. L. Andrews, *Chiral discrimination in optical trapping and manipulation*, New J. Phys. **16**, 103021 (2014).
- [22] S. B. Wang and C.T. Chan, *Lateral optical force on chiral particles near a surface*, Nat. Commun. **5**, 3307 (2014).
- [23] A. Hayat, J. B. Mueller, and F. Capasso, *Lateral chirality-sorting optical forces*, Proc. Natl. Acad. Sci. U.S.A. **112**, 13190 (2015).
- [24] M. H. Alizadeh and B. M. Reinhard, *Enhanced optical chirality through locally excited surface plasmon polaritons*, ACS Photonics **2**, 1780 (2015).
- [25] A. Canaguier-Durand and C. Genet, *Plasmonic lateral forces on chiral spheres*, J. Opt. **18**, 015007 (2016).
- [26] H. Chen, C. Liang, S. Liu, and Z. Lin, *Chirality sorting using two-wave-interference-induced lateral optical force*, Phys. Rev. A **93**, 053833 (2016).
- [27] Y. Zhao, A. A. Saleh, and J. A. Dionne, *Enantioselective optical trapping of chiral nanoparticles with plasmonic tweezers*, ACS Photonics **3**, 304 (2016).
- [28] T. Zhang, M. R. C. Mahdy, Y. Liu, J. H. Teng, C. T. Lim, Z. Wang, and C.-W. Qiu, *All-optical chirality-sensitive sorting via reversible lateral forces in interference fields*, ACS Nano **11**, 4292 (2017).
- [29] P. Acebal, L. Carretero, and S. Blaya, *Design of an optical conveyor for selective separation of a mixture of enantiomers*, Opt. Express **25**, 32290 (2017).
- [30] C.-S. Ho, A. Garcia-Etxarri, Y. Zhao, and J. Dionne, *Enhancing enantioselective absorption using dielectric nanospheres*, ACS Photonics, **4**, 197 (2017).
- [31] T. Cao and Y. Qiu, *Lateral sorting of chiral nanoparticles using Fano-enhanced chiral force in visible region*, Nanoscale **10**, 566 (2018).
- [32] M. L. Solomon, J. Hu, M. Lawrence, A. García-Etxarri, J. A. Dionne, *Enantiospecific optical enhancement of chiral sensing and separation with dielectric metasurfaces*, ACS Photonics **6**, 43 (2018).
- [33] R. J. Hernandez, A. Mazzulla, A. Pane, K. Volke-Sepulveda, and G. Cipparrone, *Attractive-repulsive dynamics on light-responsive chiral microparticles induced by polarized tweezers*, Lab Chip **13**, 459 (2013).
- [34] G. Tkachenko and E. Brasselet, *Optofluidic sorting of material chirality by chiral light*, Nat. Commun. **5**, 3577 (2014).
- [35] M. Donato, J. Hernandez, A. Mazzulla, C. Provenzano, R. Saija, R. Sayed, S. Vasi, A. Magazzu, P. Pagliusi, R. Bartolino, P. Gucciardi, O. Marago, and G. Cipparrone, *Polarization-dependent optomechanics mediated by chiral microresonators*, Nat. Commun. **5**, 3656 (2014).
- [36] G. Tkachenko and E. Brasselet, *Helicity-dependent three-dimensional optical trapping of chiral microparticles*, Nat. Commun. **5**, 4491 (2014).
- [37] Y. Zhao *et al.*, *Nanoscope control and quantification of enantioselective optical forces*, Nat. nanotechnology **12**, 1055 (2017).
- [38] G. Schnoering, L. V. Poulikakos, Y. Rosales-Cabara, A. Canaguier-Durand, D. J. Norris, and C. Genet, *Three-dimensional enantiomeric recognition of optically trapped single chiral nanoparticles*, Phys. Rev. Lett. **121**, 023902 (2018).
- [39] N. Kravets, A. Aleksanyan, and E. Brasselet, *Chiral optical Stern-Gerlach Newtonian experiment*, Phys. Rev. Lett. **122**, 024301 (2019).
- [40] N. Kravets, A. Aleksanyan, H. Chraibi, J. Leng, and E. Brasselet, *Optical enantioseparation of racemic emulsions of chiral microparticles*, Phys. Rev. App. **11**, 044025 (2019).
- [41] K. Diniz, R. S. Dutra, L. B. Pires, N. B. Viana, H. M. Nussenzveig and P. A. Maia Neto, *Negative optical torque on a microsphere in optical tweezers*, Opt. Express **27**, 5905 (2019).
- [42] A. Canaguier-Durand and C. Genet, *Chiral route to pulling optical forces and left-handed optical torques*, Phys. Rev. A **92**, 043823 (2015).
- [43] P. A. Maia Neto and H. M. Nussenzveig, *Theory of optical tweezers*, Europhys. Lett. **50**, 702 (2000).
- [44] A. Mazolli, P. A. Maia Neto, H. M. Nussenzveig, *Theory of trapping forces in optical tweezers*, Proc. R. Soc. Lond. A, **459**, 3041 (2003).
- [45] N. B. Viana, M. S. Rocha, O. N. Mesquita, A. Mazolli, P. A. Maia Neto, and H. M. Nussenzveig, *Towards absolute calibration of optical tweezers*, Phys. Rev. E **75**, 021914 (2007).
- [46] R. S. Dutra, N. B. Viana, P. A. M. Neto, and H. M. Nussenzveig, *Polarization effects in optical tweezers*, J. Opt. A **9**, 221 (2007).
- [47] F. Patti, R. Saija, P. Denti, G. Pellegrini, P. Biagioni, M. A. Iatì, and O. M. Maragò, *Chiral optical tweezers for optically active particles in the T-matrix formalism*, Sci. Rep. **9**, 29 (2019).
- [48] B. Richards and E. Wolf, *Electromagnetic diffraction in optical systems II. Structure of the image field in an aplanatic system*, Proc. R. Soc. London A **253**, 358 (1959).
- [49] P. Török, P. Varga, Z. Laczik, and G. R. Booker, *Electromagnetic diffraction of light focused through a planar interface between materials of mismatched refractive indices: an integral representation*, J. Opt. Soc. Am. A **12**, 325 (1995).
- [50] E. J. Post, *Formal structure of electromagnetics* (Dover Publications, 1997).
- [51] V. Lindell, A. H. Sihvola, S. A. Tretyakov, and A. J. Viitanen, *Electromagnetic waves in chiral and bi-isotropic media*, (Artech House, Boston, 1994).
- [52] A. Lakhtakia and V. V. Varadan, *Time-harmonic electromagnetic fields in chiral media*, (Springer-Verlag, Berlin, 1989).
- [53] C. F. Bohren, *Light scattering by an optically active sphere*, Chem. Phys. Lett. **29**, 458 (1974).
- [54] See Supplemental Material at [url] for a detailed description of the force on a core-shell nanoparticle in optical tweezers.
- [55] A. R. Edmonds, *Angular Momentum in Quantum Mechanics* (Princeton University Press, Princeton, 1957).
- [56] NIST digital library of mathematical functions. <https://dlmf.nist.gov/10.2>, Release 1.0.22 of 2019-03-15. F. W. J. Olver, A. B. Olde Daalhuis, D. W. Lozier, B. I. Schneider, R. F. Boisvert, C. W. Clark, B. R. Miller, and B. V. Saunders, eds.
- [57] R. S. Dutra, N. B. Viana, P. A. Maia Neto, and H. M. Nussenzveig, *Absolute calibration of forces in optical tweezers*, Phys. Rev. A **90**, 013825 (2014).
- [58] A. Ashkin, *Forces of a single-beam gradient laser trap on a dielectric sphere in the ray optics regime*, Biophys. J. **61**, 569 (1992).
- [59] S. Mühlig, A. Cunningham, S. Scheeler, C. Pacholski, T. Bürgi, C. Rockstuhl and F. Lederer, *Self-Assembled Plasmonic Core-Shell Clusters with an Isotropic Magnetic Dipole Response in the Visible Range*, ACS Nano **5**, 6586 (2011).

- [60] , S. N. Sheikholeslami, H. Alaeian, A. L. Koh and J. A. Dionne, *A Metafluid Exhibiting Strong Optical Magnetism*, Nano Lett. **13**, 4137 (2013).
- [61] V. Ponsinet, P. Barois, S. M. Gali, P. Richetti, J. B. Salmon, A. Vallecchi, M. Albani, A. Le Beulze, S. Gomez-Grana, E. Duguet, S. Mornet, and M. Treguer-Delapierre, *Resonant isotropic optical magnetism of plasmonic nanoclusters in visible light*, Phys. Rev. B **92**, 220414(R) (2015).
- [62] Z. Qian, S. P. Hastings, C. Li, B. Edward, C. K. McGinn, N. Engheta, Z. Fakhraai and S.-J. Park, *Raspberry-like Metamolecules Exhibiting Strong Magnetic Resonances*, ACS Nano **9**, 1263 (2015).
- [63] Li-An Wu, Wei-En Li, Ding-Zheng Lin and Yih-Fan Chen, *Three-Dimensional SERS Substrates Formed with Plasmonic Core-Satellite Nanostructures*, Scientific Reports **7**, 13066 (2017).
- [64] Y. Zhao and J. Dionne, *Response to Comment on Enantioselective optical trapping of chiral nanoparticles with plasmonic tweezers*, ACS Photonics **5**, 2535 (2018); A. J. Mastroianni, S. A. Claridge, P. Alivisatos, *Pyramidal and chiral groupings of gold nanocrystals assembled using DNA scaffolds*, J. Am. Chem. Soc. **131**, 8455 (2009).
- [65] J. Chen, J. Ng, K. Ding, K. H. Fung, Z. Lin, and C. T. Chan, *Negative optical torque*, Sci. Reports **4**, 6386 (2014).
- [66] D. Hakobyan and E. Brasselet, *Left-handed optical radiation torque*, Nat. Photonics **8**, 610 (2014).
- [67] D. Hakobyan and E. Brasselet, *Optical torque reversal and spin-orbit rotational Doppler shift experiments*, Opt. Express **23**, 31230 (2015).

Supplemental Materials: Enantioselective manipulation of chiral nanoparticles using optical tweezers

This supplement contains an expanded theoretical description of optical tweezers of particles with a chiral shell.

We consider a circularly-polarized Gaussian beam at the objective entrance port, with $\sigma = \pm 1$ denoting left-handed/right-handed polarization. The dimensionless optical force efficiency (see main text for definition in terms of the optical force) is written as

$$\mathbf{Q}(\rho, \phi, z) = \mathbf{Q}_s(\rho, \phi, z) + \mathbf{Q}_e(\rho, \phi, z). \quad (4)$$

The extinction term \mathbf{Q}_e accounts for the rate of momen-

tum removal from the incident beam, while the scattering contribution \mathbf{Q}_s corresponds to the negative of the rate of momentum carried away by the scattered field. The explicit expressions for their cylindrical components are given below as sums over multipoles of the form

$$\sum_{\ell m} (...) \equiv \sum_{\ell=1}^{\infty} \sum_{m=-\ell}^{\ell} (...)$$

-
- Scattering axial component

$$Q_{sz}(\rho, \phi, z) = -\frac{8\gamma^2}{AN} \text{Re} \sum_{\ell m} \frac{\sqrt{\ell(\ell+2)(\ell+m+1)(\ell-m+1)}}{\ell+1} \left[(A_{\ell}A_{\ell+1}^* + B_{\ell}B_{\ell+1}^*) G_{\ell,m}^{(\sigma)} G_{\ell+1,m}^{(\sigma)*} \right] \\ - \frac{8\gamma^2}{AN} \sigma \text{Re} \sum_{\ell m} \frac{(2\ell+1)}{\ell(\ell+1)} m A_{\ell} B_{\ell}^* |G_{\ell,m}^{(\sigma)}|^2$$

- Scattering radial component

$$Q_{s\rho}(\rho, \phi, z) = \frac{4\gamma^2}{AN} \sum_{\ell m} \frac{\sqrt{\ell(\ell+2)(\ell+m+1)(\ell+m+2)}}{\ell+1} \text{Im} \left\{ (A_{\ell}A_{\ell+1}^* + B_{\ell}B_{\ell+1}^*) \right. \\ \left. \left[G_{\ell,m}^{(\sigma)} G_{\ell+1,m+1}^{(\sigma)*} + G_{\ell,-m}^{(\sigma)} G_{\ell+1,-(m+1)}^{(\sigma)*} \right] \right\} - \frac{8\gamma^2}{AN} \sigma \sum_{\ell m} \frac{(2\ell+1)}{\ell(\ell+1)} \sqrt{(\ell-m)(\ell+m+1)} \left[\text{Re}(A_{\ell}B_{\ell}^*) \text{Im}(G_{\ell,m}^{(\sigma)} G_{\ell,m+1}^{(\sigma)*}) \right]$$

- Scattering azimuthal component

$$Q_{s\phi}(\rho, \phi, z) = -\frac{4\gamma^2}{AN} \sum_{\ell m} \frac{\sqrt{\ell(\ell+2)(\ell+m+1)(\ell+m+2)}}{\ell+1} \text{Re} \left\{ (A_{\ell}A_{\ell+1}^* + B_{\ell}B_{\ell+1}^*) \times \right. \\ \left. \left[G_{\ell,m}^{(\sigma)} G_{\ell+1,m+1}^{(\sigma)*} - G_{\ell,-m}^{(\sigma)} G_{\ell+1,-(m+1)}^{(\sigma)*} \right] \right\} + \frac{8\gamma^2}{AN} \sigma \sum_{\ell m} \frac{(2\ell+1)}{\ell(\ell+1)} \sqrt{(\ell-m)(\ell+m+1)} \times \text{Re}(A_{\ell}B_{\ell}^*) \text{Re}(G_{\ell,m}^{(\sigma)} G_{\ell,m+1}^{(\sigma)*})$$

- Extinction axial component

$$Q_{ez}(\rho, \phi, z) = \frac{4\gamma^2}{AN} \text{Re} \sum_{\ell m} (2\ell+1) G_{\ell,m}^{(\sigma)} \left[(A_{\ell} + B_{\ell}) G_{\ell,m}^{(\sigma)*} \right], \quad (5)$$

- Extinction radial component

$$Q_{e\rho}(\rho, \phi, z) = \frac{2\gamma^2}{AN} \text{Im} \sum_{\ell m} (2\ell+1) G_{\ell,m}^{(\sigma)} \left[(A_{\ell} + B_{\ell}) \left(G_{\ell,m+1}^{(\sigma)-} - G_{\ell,m-1}^{(\sigma)+} \right)^* \right]$$

- Extinction azimuthal component

$$Q_{e\phi}(\rho, \phi, z) = -\frac{2\gamma^2}{AN} \text{Re} \sum_{\ell m} (2\ell + 1) G_{\ell m}^{(\sigma)} \left[(A_\ell + B_\ell) \left(G_{\ell, m-1}^{(\sigma)+} + G_{\ell, m+1}^{(\sigma)-} \right)^* \right]$$

In addition to the multipole coefficients $G_{\ell m}^{(\sigma)}(\rho, \phi, z)$ defined in Eq. (3) of the main letter, we also define

$$G_{\ell, m}^{(\sigma)}(\rho, \phi, z) = \int_0^{\theta_0} d\theta \sin \theta \cos \theta_w \sqrt{\cos \theta} T(\theta) e^{-\gamma^2 \sin^2 \theta} d_{m, \sigma}^\ell(\theta_w) J_{m-\sigma}(k\rho \sin \theta) e^{i[\Phi_w(\theta) + k_w \cos \theta_w z]},$$

$$G_{\ell, m}^{(\sigma)\pm}(\rho, \phi, z) = \int_0^{\theta_0} d\theta \sin \theta \sin \theta_w \sqrt{\cos \theta} T(\theta) e^{-\gamma^2 \sin^2 \theta} d_{m\pm 1, \sigma}^\ell(\theta_w) J_{m-\sigma}(k\rho \sin \theta) e^{i[\Phi_w(\theta) + k_w \cos \theta_w z]},$$

with $\theta_w = \sin^{-1}(\sin \theta / N)$ and $N = n_w / n_g$. The phase Φ_w accounts for the spherical aberration arising from the refractive index mismatch at the glass-water interface:

$$\Phi_w(\theta) = k(-L/N \cos \theta + NL \cos \theta_w),$$

where L represents the distance between the paraxial focal plane and the glass slide. We also take $T(\theta) = \frac{2 \cos \theta}{\cos \theta + N \cos \theta_w}$ for the Fresnel transmission amplitude (neglecting polarization dependence since $N \approx 1$).

The factor

$$A = 16\gamma^2 \int_0^{s_0} ds s \exp(-2\gamma^2 s^2) \frac{\sqrt{(1-s^2)(N^2-s^2)}}{(\sqrt{1-s^2} + \sqrt{N^2-s^2})^2}$$

is the fraction of beam power transmitted into the sample chamber, with $s_0 = \text{NA}/n_g$.

The optical force components also depend on the effective external Mie coefficients A_ℓ and B_ℓ which we derive as follows:

$$\begin{aligned} A_\ell &= a_\ell + i\sigma d_\ell \\ B_\ell &= b_\ell - i\sigma c_\ell. \end{aligned} \quad (6)$$

A_ℓ and B_ℓ are convenient for a number of applications involving circularly-polarized fields scattered by chiral media. The coefficients a_ℓ , b_ℓ , c_ℓ and d_ℓ are the external Mie coefficients for a sphere made of chiral material [1]. For a core-shell nanosphere, their explicit expressions [2] are given in terms of the size parameters $\alpha = k_w a$ and $v = k_w r$ corresponding to the core and outer radii a and r . The refractive indexes of the chiral shell (with respect to the host) are $N_{L/R} = (\sqrt{\epsilon\mu} \pm \kappa)/n_w$, where κ is the chirality parameter (see main text). We also need the relative refractive index of the core N_I with respect to the host medium of index n_w . Finally, $N_{II} = (N_L + N_R)/2$ is the average relative index of the chiral shell.

$$\begin{aligned} a_\ell &= -\Delta_\ell^{-1}(A_{R\ell}W_{L\ell} + A_{L\ell}W_{R\ell}) \\ b_\ell &= -\Delta_\ell^{-1}(B_{L\ell}V_{R\ell} + B_{R\ell}V_{L\ell}) \\ c_\ell &= i\Delta_\ell^{-1}(A_{L\ell}V_{R\ell} - A_{R\ell}V_{L\ell}) \\ d_\ell &= i\Delta_\ell^{-1}(B_{R\ell}W_{L\ell} - B_{L\ell}W_{R\ell}) \end{aligned}$$

with

$$\begin{aligned} \Delta_\ell &= W_{L\ell}V_{R\ell} + B_{L\ell}W_{R\ell} \\ A_{R\ell} &= X_{R\ell}(-)\eta_\ell^{(1)}(v) - N_{II}U_{R\ell}(-)j_\ell(v) \\ A_{L\ell} &= X_{L\ell}(+)\eta_\ell^{(1)}(v) - N_{II}U_{L\ell}(+)j_\ell(v) \\ B_{L\ell} &= X_{L\ell}(-)N_{II}\eta_\ell^{(1)}(v) - U_{L\ell}(-)j_\ell(v) \\ B_{R\ell} &= X_{R\ell}(+)N_{II}\eta_\ell^{(1)}(v) - U_{R\ell}(+)j_\ell(v) \\ V_{L\ell} &= X_{L\ell}(+)\eta_\ell^{(3)}(v) - N_{II}U_{L\ell}(+)h_\ell^{(1)}(v) \\ V_{R\ell} &= X_{R\ell}(-)\eta_\ell^{(3)}(v) - N_{II}U_{R\ell}(-)h_\ell^{(1)}(v) \\ W_{L\ell} &= X_{L\ell}(-)N_{II}\eta_\ell^{(3)}(v) - U_{L\ell}(-)h_\ell^{(1)}(v) \\ W_{R\ell} &= X_{R\ell}(+)N_{II}\eta_\ell^{(3)}(v) - U_{R\ell}(+)h_\ell^{(1)}(v) \end{aligned}$$

We have also introduced the functions

$$\begin{aligned} X_{R\ell}(\pm) &= j_\ell(N_R v) + D_{4\ell}y_\ell(N_R v) \pm D_{2\ell}y_\ell(N_L v) \\ X_{L\ell}(\pm) &= j_\ell(N_L v) + D_{1\ell}y_\ell(N_L v) \pm D_{3\ell}y_\ell(N_R v) \\ U_{R\ell}(\pm) &= \eta_\ell^{(1)}(N_R v) + D_{4\ell}\eta_\ell^{(2)}(N_R v) \pm D_{2\ell}\eta_\ell^{(2)}(N_L v) \\ U_{L\ell}(\pm) &= \eta_\ell^{(1)}(N_L v) + D_{1\ell}\eta_\ell^{(2)}(N_L v) \pm D_{3\ell}\eta_\ell^{(2)}(N_R v) \end{aligned}$$

where

$$\begin{aligned} D_{1\ell} &= -\Delta_\ell^{-1}[G_\ell(N_R)H_\ell(N_L) + F_\ell(N_R)K_\ell(N_L)] \\ D_{2\ell} &= \Delta_\ell^{-1}[F_\ell(N_R)K_\ell(N_R) - G_\ell(N_R)H_\ell(N_R)] \\ D_{3\ell} &= \Delta_\ell^{-1}[G_\ell(N_L)H_\ell(N_L) - F_\ell(N_L)K_\ell(N_L)] \\ D_{4\ell} &= -\Delta_\ell^{-1}[G_\ell(N_L)H_\ell(N_R) + F_\ell(N_L)K_\ell(N_R)] \end{aligned}$$

F, G, H and K are functions of the refractive index variable $N = N_L, N_R$ defined as

$$\begin{aligned} F_\ell(N) &= N_{II}y_\ell(N\alpha)\eta_\ell^{(1)}(N_I\alpha) - N_I\eta_\ell^{(2)}(N\alpha)j_\ell(N_I\alpha) \\ G_\ell(N) &= N_Iy_\ell(N\alpha)\eta_\ell^{(1)}(N_I\alpha) - N_{II}\eta_\ell^{(2)}(N\alpha)j_\ell(N_I\alpha) \\ H_\ell(N) &= N_Ij_\ell(N\alpha)\eta_\ell^{(1)}(N_I\alpha) - N_I\eta_\ell^{(1)}(N\alpha)j_\ell(N_I\alpha) \\ K_\ell(N) &= N_{II}j_\ell(N\alpha)\eta_\ell^{(1)}(N_I\alpha) - N_{II}\eta_\ell^{(1)}(N\alpha)j_\ell(N_I\alpha) \end{aligned}$$

$j_\ell(\rho)$, $y_\ell(\rho)$ are the spherical Bessel functions of the first and second kind, respectively; whereas $h_\ell^{(1)}(\rho)$ is the spherical Hankel function of the first kind [3]. We also define

$$\begin{aligned}\eta_\ell^{(1)}(\rho) &= \frac{1}{\rho} d[\rho j_\ell(\rho)]/d\rho \\ \eta_\ell^{(2)}(\rho) &= \frac{1}{\rho} d[\rho y_\ell(\rho)]/d\rho \\ \eta_\ell^{(3)}(\rho) &= \frac{1}{\rho} d[\rho h_\ell^{(1)}(\rho)]/d\rho\end{aligned}$$

-
- [1] C. F. Bohren and D. R. Huffman, *Absorption and Scattering of Light by Small Particles* (Wiley, New York, 1983).
[2] C. F. Bohren, Scattering of electromagnetic waves by an optically active spherical shell, J. Chem. Phys. **62**, 1566 (1975).
[3] NIST digital library of mathematical functions. <https://dlmf.nist.gov/10.47#E3>, Release 1.0.16 of 2017-09-18. F. W. J. Olver, A. B. Olde Daalhuis, D. W. Lozier, B. I. Schneider, R. F. Boisvert, C. W. Clark, B. R. Miller, and B. V. Saunders, eds.